



The role of oceanic ventilation and terrestrial outflow in atmospheric non-methane hydrocarbons over the Chinese marginal seas

Jian Wang¹, Lei Xue², Qian Yao Ma¹, Feng Xu¹, Gaobin Xu¹, Shibo Yan¹, Jiawei Zhang³, Jianlong Li¹,
Honghai Zhang¹, Guiling Zhang¹, and Zhaohui Chen⁴

¹Frontiers Science Center for Deep Ocean Multispheres and Earth System, Key Laboratory of Marine Chemistry Theory and Technology, Ministry of Education, and College of Chemistry and Chemical Engineering, Ocean University of China, Qingdao 266100, China

²Department of Chemistry, College of Environmental Science and Forestry, State University of New York, Syracuse, NY, 13210, United States

³Eco-Environmental Monitoring and Research Center, Pearl River Valley and South China Sea Ecology and Environment Administration, Ministry of Ecology and Environment, Guangzhou 510610, China

⁴Key Laboratory of Physical Oceanography, Ministry of Education, Ocean University of China, Qingdao 266100, China

Correspondence: Honghai Zhang (honghaizhang@ouc.edu.cn)

Received: 6 December 2023 – Discussion started: 6 March 2024
Revised: 16 June 2024 – Accepted: 21 June 2024 – Published: 8 August 2024

Abstract. Non-methane hydrocarbons (NMHCs) in the marine atmosphere have been studied extensively due to their important roles in regulating atmospheric chemistry and climate. However, very little is known about the distribution and sources of NMHCs in the lower atmosphere over the marginal seas of China. Herein, we characterized the atmospheric NMHCs (C₂–C₅) in both the coastal cities and the marginal seas of China in the spring of 2021, with a focus on identifying the sources of NMHCs in the coastal atmosphere. The NMHCs in urban atmospheres, especially alkanes, were significantly higher compared to those in the marine atmosphere, suggesting that terrestrial NMHCs may be an important reservoir/source in the marine atmosphere. A significant correlation was observed between the alkane concentrations and the distances from sampling sites to the nearest land or retention of air mass over land, indicating that alkanes in the marine atmosphere are largely influenced by terrestrial inputs through air mass transport. For alkenes, a greater impact from oceanic emissions was determined due to the lower terrestrial concentrations, short atmospheric lifetime, and substantial sea-to-air fluxes of alkenes compared to alkanes (489 ± 454 vs. 129 ± 106 nmol m⁻² d⁻¹). As suggested by the positive matrix factorization, terrestrial inputs contributed to 89 % of alkanes and 69.6 % of alkenes in Chinese marginal seas, subsequently contributing to 84 % of the ozone formation potential associated with C₂–C₅ NMHCs. These findings underscore the significance of terrestrial outflow in controlling the distribution and composition of atmospheric NMHCs in the marginal seas of China.

1 Introduction

Non-methane hydrocarbons (NMHCs), a significant subset of volatile organic compounds (VOCs), are acknowledged as key precursors to tropospheric ozone formation (Houweling et al., 1998; Solomon et al., 2005) and organic aerosol generation (Hallquist et al., 2009; Wu and Xie, 2018), playing a pivotal role in atmospheric chemistry. The presence and activity of NMHCs in the troposphere have far-reaching implications, not only influencing the dynamics of ozone and organic aerosol formation but also significantly impacting air quality. These compounds are intricately linked to heightened human health risks and have indirect yet profound effects on the broader climate system through their interactions with various atmospheric processes (Yuan et al., 2018).

The emission of NMHCs into the atmosphere stems from an array of natural and anthropogenic processes. Oceanic sources of NMHCs predominantly entail the biogenic production of phytoplankton and photochemical degradation of dissolved organic matter (DOM) (Bonsang et al., 1992; Li et al., 2019; Riemer et al., 2000; Sahu et al., 2010). However, they are minimal when compared to terrestrial inputs. Despite the uncertainties in the global flux of VOCs, substantial evidence indicates a significant discrepancy between terrestrial emissions ($660\text{--}1146\text{ Tg C yr}^{-1}$) (Guenther et al., 1995, 2012; Messina et al., 2016; Sindelarova et al., 2014; Singh and Zimmerman, 1992) and marine emissions ($5\text{--}36\text{ Tg C yr}^{-1}$) (Guenther et al., 1995; Singh and Zimmerman, 1992). A substantial amount of NMHCs originating from terrestrial sources (e.g., vehicular emissions, biomass combustion, industrial activities, and continental vegetation emissions) can be transported into the offshore atmosphere via air mass conveyance (Wang et al., 2005; Kato et al., 2007; Song et al., 2020). Subsequently, these supplementary terrestrial NMHCs will play a pivotal role in shaping the chemical composition of the offshore atmosphere and influencing local environmental dynamics. Hence, to further understand the characteristics, variation, and origins of NMHCs in the offshore atmosphere, it is imperative to scrutinize oceanic emissions, and it is simultaneously necessary to ascertain the effect of terrestrial outflow on nearshore NMHCs.

The Yellow Sea and the East China Sea are important parts of Chinese marginal seas, situated along the densely populated and industrialized eastern coast of China. The rapid pace of Chinese development has seen a notable escalation of anthropogenic NMHC emissions over recent decades (He et al., 2019). Presently, excessive NMHC emissions and severe ozone pollution have emerged as urgent environmental challenges in China, particularly in highly urbanized and industrialized areas along the eastern coast (Liu et al., 2016; Zhang et al., 2018). The seasonal cycle of the Asian monsoon and diurnal fluctuations in sea–land breezes can facilitate the transport of terrestrial pollution to the marine atmosphere (Ding et al., 2004; Wang et al., 2003; Talbot et al., 2003; Russo et al., 2003). Additionally, eutrophication in coastal

regions fosters the proliferation of phytoplankton, potentially augmenting the natural emissions of NMHCs. Consequently, conducting atmospheric investigations in the coastal region of eastern China is effective in revealing the potential effects of land–sea interactions on offshore atmospheric NMHCs.

In the spring of 2021, atmospheric samples were systematically collected from both coastal cities and marginal seas of China, providing representative insights into the characteristics of NMHCs (C₂–C₅) and facilitating discussion on the interplay between ocean emissions and terrestrial outflow concerning atmospheric NMHCs. Ultimately, the contributions of diverse sources to NMHCs were quantified using the positive matrix factorization (PMF) model, with assistance from indications provided by other typical gases, mainly dimethyl sulfur (DMS), volatile halogenated compounds (VHCs), and monocyclic aromatics.

2 Methods

2.1 Sample collection

Urban samples were collected from eight coastal cities in China from 27 March to 1 April 2021 (Fig. 1). Air samples were collected using fused silica-lined canisters (2.5 L), which were cleaned three times via a canister cleaning system (2101DS, Nutech), and pumped into a negative pressure state before sampling. The sampling sites were selected at the top of high buildings to minimize contamination of particular point sources. Air samples were collected at 09:00 and 21:00 local time (UTC+8) to represent the urban atmospheric conditions during the day and night, respectively. Note that nighttime samples in Xiamen and Qinzhou were missing.

Oceanic air samples were collected aboard R/V *Dong Fang Hong 3* during the voyage in the Yellow Sea and the East China Sea from 17 April to 2 May 2021. A total of 19 oceanic air samples were collected on the top deck facing the wind when the ship was about to arrive at the station and started to slow down. Seawater samples were collected via prewashed Niskin bottles (12 L) incorporated into a conductivity–temperature–depth rosette sensor (Seabird 911). Sampling details for urban (Table S4) and marine samples (Table S5) are shown in the tables in the Supplement.

2.2 Analysis of air samples

For the measurement of most types of gases, air samples were processed immediately after being brought back to the laboratory, using an atmospheric pre-concentrator system (8900DS, Nutech) coupled with a gas chromatograph–mass selective detector (GC-MSD) system (GC-7890A, MSD-5975, Agilent). The pretreatments of air samples were as follows. First, the atmospheric pre-concentrator system was baked for 10 min to clean the interior instrument. Then, trap 1 was cooled to $-170\text{ }^{\circ}\text{C}$ using liquid N₂, and a 300 mL air

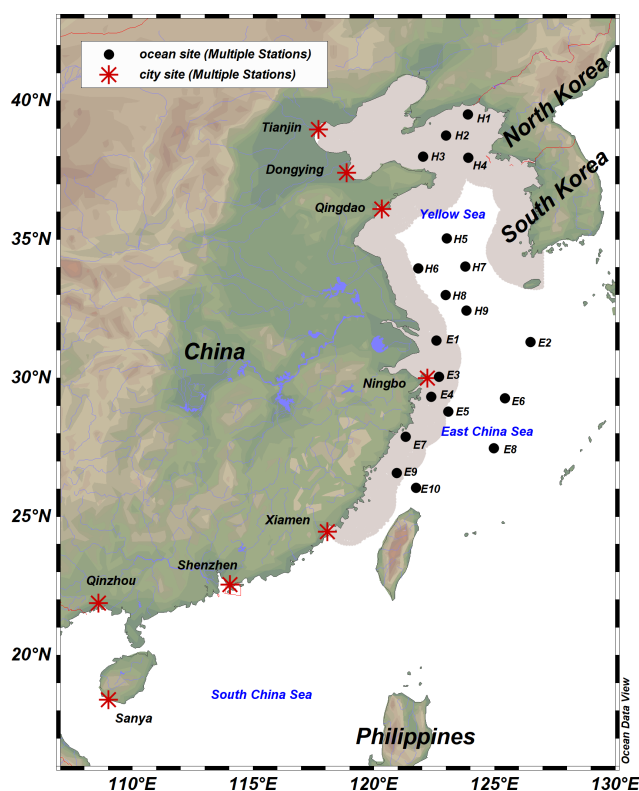


Figure 1. Map showing the sampling stations in the coastal cities (red asterisks) and marginal seas (black dots) of China from March to May 2021. The gray-shaded area represents the inshore region within 100 km from the coastline (Schlitzer, 2023).

sample was pumped from the canister into trap 1 for the initial concentration of the target compounds, while N_2 and O_2 escaped due to their lower boiling points. After trap 2 was cooled to $-50\text{ }^\circ\text{C}$, trap 1 was heated to $30\text{ }^\circ\text{C}$ to transfer the target compounds from trap 1 to trap 2. Moisture and CO_2 were removed in the second concentration. Then, trap 2 was warmed up to transfer the target compounds into the last trap for cryofocusing ($-175\text{ }^\circ\text{C}$). Finally, the last trap was instantaneously heated to $200\text{ }^\circ\text{C}$ via gas bath heating, and the target compounds were delivered into the GC-MSD system by ultra-pure He.

For the parameter settings of GC-MSD, the temperature of the inlet, quadrupole, and ionization source was 150, 150, and $230\text{ }^\circ\text{C}$, respectively. The inlet was set to split mode with a ratio of 10 : 1. The flow rate of the carrier gas (He) was set to 1.5 mL min^{-1} in the instant-flow mode. Specific columns were selected to separate the NMHCs (Rt-Alumina BOND/KCl, Restek), monocyclic aromatics (DB-624, Agilent), DMS (CP7529, Agilent), and VHCs (DB-624, Agilent). Gas standards of NMHCs in N_2 (Linde Gas, Germany) were diluted to 0.1–1 ppb for identification and calibration. Details of temperature programming and detector parameters can be seen in Zou et al. (2021) and Li et al. (2019). The precision and detection limits for the trace gases in the

present study were 1 %–7 % and 0.03–20.0 ppt, respectively (Table S1 in the Supplement). Specifically, carbon monoxide (CO) was analyzed on site using a trace gas analyzer (TA3000R, Ametek) with a lower detection limit of 10 ppb; more details can be found in Xu et al. (2023). Note that data on DMS, CO, and VHCs from marine atmospheric samples were graciously provided by colleagues in the same laboratory. These data were used only as supporting information in the interpretation of our core dataset in this paper (e.g., correlation analysis).

2.3 Analysis of seawater samples

C2–C5 NMHCs in seawater were measured immediately on board using a purge and trap system coupled with the gas chromatography equipped with a flame ionization detector (GC-FID; 7890B, Agilent). The purge and trap system was improved based on a previously self-designed device described by Li et al. (2019). Briefly, seawater was collected using a customized glass sampler (500 mL) and connected to the inlet of the system. Then, seawater was transformed into the extraction cell under the pressure of pure N_2 and purged with pure- N_2 bubble flow (250 mL min^{-1}). The moisture of the carrier gas condensed in a thin glass tube that was placed in a cold chamber ($4\text{--}6\text{ }^\circ\text{C}$), and the carbon dioxide was absorbed by a glass tube filled with Ascarite II (Merck). The targets were concentrated in a passivated stainless-steel tube immersed in liquid nitrogen for 26 min. Then, the steel tube was heated by boiling water, and the six-way valve was turned immediately for the inlet situation. The concentrated target compounds were transferred into the Rt-Alumina BOND/KCl capillary column for separation and were determined by FID. The parameters of the inlet, oven, and detector are shown in Table S2. The gas standard (Linde Gas, Germany) was diluted with ultra-pure N_2 to 10 ppb for identification and quantification. The instrumental blank was made to guarantee data reliability. The precision and detection limits were 3 %–6 % and $0.5\text{--}1.0\text{ pmol L}^{-1}$ (Table S3).

2.4 Calculation of sea-to-air flux

The sea-to-air flux of each NMHC (F , $\text{nmol m}^{-2}\text{ d}^{-1}$) was calculated using Eq. (1):

$$F = k \times (C_w - C_a \times H), \quad (1)$$

where k (m s^{-1}) is the gas transfer velocity described by Eq. (2); H is Henry's law constant; and C_w (pmol L^{-1}) and C_a (ppb) are concentrations of each NMHC in the surface seawater (5 m depth) and atmosphere, respectively.

$$k = 0.31 \times u^2 \times \left(\frac{Sc}{660} \right)^{-0.5} \quad (2)$$

Here, u (m s^{-1}) is the wind velocity at 10 m. Sc is the Schmidt number, defined as $Sc = \nu/D$, and ν is the kine-

matic viscosity of seawater calculated by Eq. (3) (Wan-ninkhof, 1992). D is the gas diffusion coefficient related to temperature and described by Eq. (4) (Wilke and Chang, 1955).

$$v = 1.052 + 1.300 \times 10^{-3} \times t + 5.000 \times 10^{-6} \times t^2 + 5.000 \times 10^{-7} \times t^3 \quad (3)$$

$$D = \frac{7.4 \times 10^{-8} (q \times M_b)^{0.5} \times T}{n_b \times V_a^{0.6}} \quad (4)$$

Here, t ($^{\circ}$) is the degree Celsius of seawater, q is the association factor of water, M_b (g mol^{-1}) is the molar weight of water, T (K) is the degree Kelvin of seawater, n_b is the dynamic viscosity of seawater, and V_a is the molar volume at the boiling point.

2.5 Calculation of OFP and P_{SOAP} of NMHCs

To assess the environmental implications of NMHCs, the ozone formation potential (OFP; $\mu\text{g m}^{-3}$) and secondary organic aerosol (SOA) formation potential (P_{SOAP} ; $\mu\text{g m}^{-3}$) are calculated using Eqs. (5) and (6), respectively (Carter, 1994):

$$\text{OFP}_i = \text{MIR}_i \times C_i, \quad (5)$$

$$P_{\text{SOAP}_i} = \sum C_i \times \text{SOAP}_i \times \text{FAC}_{\text{toluene}}/100, \quad (6)$$

where C_i represents the concentration of NMHCs; MIR_i ($\text{g O}_3/\text{g VOCs}$) and SOAP_i (relative to toluene = 100) are constants that represent the maximum incremental reactivity and SOA potential of i , respectively (Carter, 2010); and $\text{FAC}_{\text{toluene}}$ is the fractional aerosol coefficient of toluene, which has a value of 5.4% (Grosjean and Seinfeld, 1989). Specific data are listed in Table S11.

2.6 Normalized concentrations and lifetime-weighted concentrations of NMHCs

To effectively compare the NMHC variation with respect to the distance from the sampling sites to land (see Fig. 2d, f), we calculated the normalized concentration for each NMHC ($C_{\text{Nor-}i}$) using Eq. (7):

$$C_{\text{Nor-}i} = \frac{C_i}{C_{\text{max-}i}}, \quad (7)$$

where C_i is the concentration of gas i , and $C_{\text{max-}i}$ is the maximum of gas i .

A novel approach was employed to analyze the correlation between the concentrations of various NMHCs and their sea-to-air fluxes. Concentrations were weighted according to the respective atmospheric $\bullet\text{OH}$ lifetime of each NMHC. This was achieved by dividing the concentration of each NMHC by its corresponding atmospheric $\bullet\text{OH}$ lifetime, yielding a

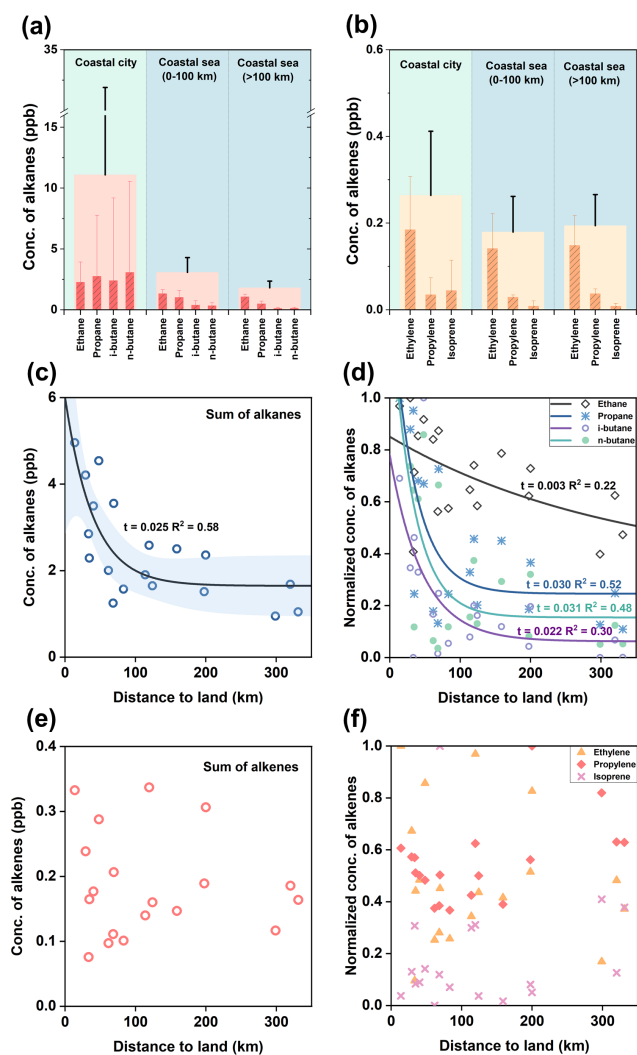


Figure 2. Means of the concentrations of alkanes (a) and alkenes (b) in the atmosphere over coastal cities ($n = 14$) as well as nearshore (0–100 km, $n = 10$) and offshore (> 100 km, $n = 9$) coastal seas of China. The wider columns in panels (a) and (b) represent the sums of individual alkanes and alkenes, respectively, with error bars depicting the propagated errors from each NMHC. Summed alkane (c) and alkene (e) and normalized concentrations of specific alkane (d) and alkene (f) plotted as a function ($y = Ae^{-tx} + y_0$) of the distance from the sampling sites to the nearest land.

“lifetime-weighted concentration” for each NMHC ($C_{\text{life-}i}$) (Eq. 8). This method provides a more nuanced understanding of the impact of oceanic emissions on NMHCs, taking into account not only their abundance but also their residence in the atmosphere.

$$C_{\text{life-}i} = \frac{C_i}{\tau_i} \quad (8)$$

Here, C_i is the atmospheric concentration of gas i , and τ_i is the $\bullet\text{OH}$ lifetime of gas i . The approximate atmospheric

lifetime of each NMHC was calculated assuming an average $[\bullet\text{OH}]$ of $6 \times 10^5 \text{ molec. cm}^{-3}$ within 24 h at 288 K (Jobson et al., 1999), with specific data listed in Table 1.

2.7 Calculation of the shortest distance from the sampling station to land

Coastline latitude and longitude data near the study area (20–45° N, 110–130° E) were extracted from the World Vector Shoreline (Wessel and Smith, 1996). Subsequently, distances from the maritime sampling stations to all coastal locations were computed. The minimum value among these distances was selected as the shortest distance to land (listed in Table S9).

2.8 Calculation of retention of air mass over land

To identify whether an air mass was mainly from terrestrial or oceanic regions, the retention ratio of the air mass over land (R_L) was calculated by Eq. (9):

$$R_L = \frac{\sum_{n=1}^{N_{\text{land}}} e^{-\frac{t_n}{48}}}{\sum_{n=1}^{N_{\text{total}}} e^{-\frac{t_n}{48}}}, \quad (9)$$

where N_{total} is the total number of trajectory endpoints (Stein et al., 2015). N_{land} is the total number of trajectory endpoints located over land, while t_n is the backward tracking time in units of hours, and $e^{-\frac{t_n}{48}}$ is the weighting factor related to tracking time as the diffusion of air mass takes place along the transport path rather than in the nearby regions. As a result, the larger R_L value indicates that the air mass is more influenced by terrestrial transport, and its source is more likely to be on land. Similar methods have been used to calculate the average residence time of sampled air masses in the Arctic (Willis et al., 2017) and identify the percentage of time spent by trajectories over different surface types in the Antarctic (Decesari et al., 2020). R_L values were calculated by three different timescale trajectories (48, 72, and 96 h) (listed in Table S9). The mean R_L ($n = 3$) was finally applied to analyze the terrestrial influence on oceanic NMHCs, mitigating the uncertainty caused by the trajectory with different timescales.

2.9 Application of the PMF model

The PMF model, introduced in detail in the study of Paatero and Tapper (1994), was applied to analyze the data of atmospheric NMHCs in the Yellow Sea and the East China Sea. Based on a matrix consisting of the concentrations of diverse chemical species, the objective of PMF is to determine the number of NMHC source factors, the chemical composition profile of each factor, and the contribution of each factor to species. The matrix representation of this model is (Eq. 10)

$$x_{ij} = \sum_{k=1}^p g_{ik} f_{kj} + e_{ij}, \quad (10)$$

where x_{ij} represents the concentration of species j measured on sample i , and p denotes the number of factors facilitating the samples. f_{kj} represents the concentration of species j in factor profile k , g_{ik} denotes the relative contribution of factor k to sample i , and e_{ij} represents the PMF model error of species j measured on sample i . The factors resolved by PMF are typically interpreted as sources. The objective of this algorithm is to find the values of f_{kj} , g_{ik} , and p that best reproduce x_{ij} , continuously adjusting f_{kj} and g_{ik} until the minimum Q value for a given p is attained. Q is defined as Eq. (11):

$$Q = \sum_{i=1}^n \sum_{j=1}^m \left(\frac{e_{ij}}{\sigma_{ij}} \right)^2, \quad (11)$$

where σ_{ij} represents the uncertainty in the concentration of species j in sample i , n is the number of samples, and m is the number of species. In applying the PMF model, the significance of missing data in the matrix was decreased by using the species median. The uncertainty for normal data was estimated as 20 % of the NMHC concentrations because the analytical uncertainty was not available (Buzcu and Fraser, 2006). The model was run 20 times, and we selected the result with the minimum Q value. Additionally, scaled residuals are instrumental in assessing the fit of the PMF model to the observed data. They represent the difference between the observed and modeled data, scaled by the uncertainty in the observed data. In this PMF analysis, approximately 94 % of the scaled residuals ranged from -3 to 3 (Fig. S1), suggesting a reasonable fit of the model result.

3 Results and discussion

3.1 Atmospheric concentrations of NMHCs in coastal cities and marginal seas of China

To clarify, NMHCs determined in this study were separated into two groups for further discussion based on their distinctly different atmospheric reactivity and lifetimes: alkanes (long lifetime, 8.2–78 d) and alkenes (short lifetime, 0.19–2.3 d). In the urban atmosphere ($n = 14$), the mean (range) concentration of ethane, propane, i-butane, and n-butane was 2.26 ± 1.66 (0.277–5.72), 2.95 ± 5.12 (0.149–20.1), 2.57 ± 6.99 (BD–27.6), and 3.29 ± 7.68 (0.018–30.2) ppb, respectively (Table 1). Alkanes combined accounted for $\sim 76\%$ – 99% of total NMHCs measured in this study, which agrees with previous studies reporting alkanes as the dominant NMHCs in the urban atmosphere of China, e.g., 43.7 % (Song et al., 2007) and $> 50\%$ (Li et al., 2015). For alkene species in the urban atmosphere ($n = 14$), the mean (range) of ethylene, propylene, and isoprene was 0.180 ± 0.126 (0.035–0.390), 0.036 ± 0.040 (BD–0.129), and 0.046 ± 0.072 (0.006–0.250) ppb, respectively.

Similarly, alkanes were also dominant components in the marine atmosphere, accounting for $\sim 86\%$ – 95% of

Table 1. Atmospheric and seawater concentrations, sea-to-air fluxes, and the calculated atmospheric lifetime of each NMHC based on the reaction with hydroxyl radicals ($\bullet\text{OH}$).

Species	Conc. in urban air (ppb)	Conc. in oceanic air (ppb)	Conc. in seawater (pmol L^{-1})	Sea-to-air flux ($\text{nmol m}^{-2} \text{d}^{-1}$)	Atmospheric lifetime ^b (d)
Ethane	2.26 (0.277–5.72)	1.24 (0.686–1.72)	11.6 (4.70–22.8)	44.6 (0.2–118)	78
Propane	2.95 (0.149–20.1)	0.822 (0.226–1.79)	12.6 (3.68–136)	41.5 (0.2–157)	18
i-Butane	2.57 (BD ^a –27.6)	0.283 (BD–1.17)	9.46 (1.54–35.3)	31.7 (0.1–146)	9.1
n-Butane	3.29 (0.018–30.2)	0.256 (0.025–0.694)	4.95 (BD–32.9)	10.9 (–0.8–96.1)	8.2
Ethylene	0.180 (0.035–0.390)	0.151 (0.028–0.295)	70.4 (8.40–136)	321 (1.7–775)	2.3
Propylene	0.036 (BD–0.129)	0.033 (0.022–0.060)	15.2 (2.42–27.6)	56.1 (0.2–212)	0.73
Isoprene	0.046 (0.006–0.250)	0.008 (BD–0.043)	31.0 (3.43–105)	112 (0.5–468)	0.19

^a Below the detection limit. ^b Assuming an average $[\bullet\text{OH}]$ of $6 \times 10^5 \text{ molec. cm}^{-3}$ within 24 h (Jobson et al., 1999) and using the rate constant with $\bullet\text{OH}$ at 288 K taken from Atkinson et al. (1997).

NMHCs. In the marine atmosphere ($n = 19$), the mean (range) concentration of ethane, propane, i-butane, n-butane, ethylene, propylene, and isoprene was 1.24 ± 0.298 (0.686–1.72), 0.822 ± 0.518 (0.226–1.79), 0.283 ± 0.302 (BD–1.17), 0.256 ± 0.214 (0.025–0.694), 0.151 ± 0.077 (0.028–0.295), 0.033 ± 0.009 (0.022–0.060), and 0.008 ± 0.010 (BD–0.043) ppb, respectively. These values were comparable to those reported in the Bay of Bengal (Sahu et al., 2011) and the northwestern Pacific Ocean (Li et al., 2019) (Table S6). Alkanes in the urban atmosphere were on average more than 4 times higher than those in the marine atmosphere, while no significant difference was observed for concentrations of alkenes between urban and marine air ($t = 2.224$, $p = 0.156$) (Fig. 2a, b). In spatial terms, multiple NMHCs (e.g. ethane, propane, i-butane, n-butane, and ethylene) showed higher atmospheric concentrations in regions closer to land. The elevated concentrations were primarily concentrated along the coastal regions of the East China Sea and the north Yellow Sea (Fig. S3). The disparity in NMHC concentrations between land and ocean, as well as the distribution pattern of NMHCs in the marine atmosphere, suggested a potential influence of terrestrial sources on the oceanic NMHCs.

3.2 Atmospheric NMHC variability vs. estimated lifetime

The standard deviation of the natural logarithm of the NMHC mixing ratios ($S_{\ln x}$) was established to correlate to their $\bullet\text{OH}$ lifetime (τ) in the atmosphere following an exponential function of $S_{\ln x} = A\tau^{-b}$ (Jobson et al., 1998), where A and b are fitting parameters. A b value approaching 0 suggests that the NMHC variability is primarily controlled by local emission fluctuations, while a b value of 1 indicates the minimal impact of local emissions, with the variability predominantly controlled by the extent of photochemical reactions.

Employing the analytical framework in Jobson et al. (1998), we analyzed our atmospheric NMHC data from urban areas and the Chinese marginal seas. The derived b value for urban areas was 0.05 (Fig. 3a), suggesting that atmospheric NMHCs in coastal cities were mainly controlled

by local emissions. In the marine atmosphere, the b value was 0.26 (Fig. 3b), which was comparable to values reported for Gosan (0.30) (Wong et al., 2007) and continental outflow from southern China (0.31) (Wang et al., 2005), but it was significantly lower than the values for Ogasawara (0.43) (Kato et al., 2004), the northwestern Indian Ocean (0.40) (Warneke and de Gouw, 2001), and the South China Sea (0.42) (Wang et al., 2005). The b value of 0.26 in the atmosphere over the Chinese marginal seas suggests that the NMHC composition in the nearshore atmosphere is influenced by both the local oceanic emissions and the remote sources from the continent. As sites closer to the source position tend to have lower b values, the Yellow Sea and the East China Sea experience a more pronounced influence from terrestrial pollution sources compared to Ogasawara, the South China Sea, and the northwestern Indian Ocean.

3.3 Terrestrial influence on marine atmospheric NMHC variation

Given the discernible impact of terrestrial input on the spatial distributions and variabilities of marine atmospheric NMHCs, we further elucidated the role of terrestrial outflow in shaping marine atmospheric NMHC levels. This examination focused on three key factors: distance from the sampling site to land, retention of air mass over land, and transport time of air mass.

3.3.1 Distance from the sampling site to land

The distances from the oceanic sampling sites to the nearest land spanned 13.9 to 331 km, with an average of 123 km (Table S9). Significant correlations were observed between the distances and concentrations of ethane ($r = -0.553$, $n = 19$, $p = 0.014$), propane ($r = -0.605$, $n = 19$, $p = 0.006$), i-butane ($r = -0.513$, $n = 19$, $p = 0.025$), and n-butane ($r = -0.573$, $n = 19$, $p = 0.010$). When plotted against the distances, the concentrations of alkanes combined decreased with increasing distance (Fig. 2c), and different species ex-

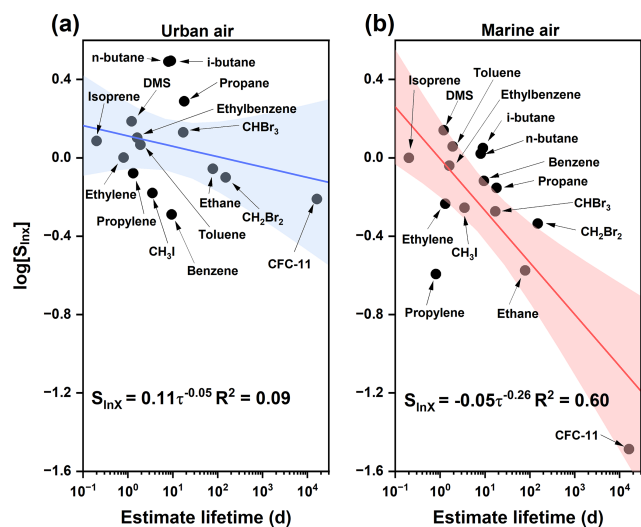


Figure 3. Atmospheric variability ($\log[S_{inX}]$) plotted as a function of the estimated \bullet OH lifetime for each NMHC from the coastal cities (a) and marginal seas of China (b). The blue and red lines are the best linear fit. The shadowed area represents the confidence band at a 95 % confidence level.

hibited distinctly specific decreasing rates (Fig. 2d). Since the concentrations between different NMHC species varied considerably, the normalized concentrations were employed to fit an attenuation equation ($y = Ae^{-tx} + y_0$) for each species. As shown in Fig. 2d, the attenuation coefficients for ethane, propane, i-butane, and n-butane are 0.003, 0.030, 0.031, and 0.022, respectively. These coefficients were correlated with their atmospheric reactivities. Species with lower reactivity and longer lifetimes, such as ethane (with a lifetime of 78 d), have the lowest attenuation coefficient. This implies that long-lifetime species could be affected by the terrestrial input even at a more remote marine site. Terrestrial influences on propane, i-butane, and n-butane were discernible only in areas much closer to land, as their concentrations stabilized at low values beyond a distance of around 100 km (Fig. 2d).

3.3.2 Retention of air mass over land

A larger retention of air mass over land (R_L) has previously been suggested to serve as an indicator of a greater terrestrial influence (Zhou et al., 2021). To mitigate the uncertainty derived from varying timescale trajectories, we calculated R_{L-mean} based on 48, 72, and 96 h backward trajectories. R_{L-mean} ranged from 0.10 to 0.96 (Table S9). When plotted against R_{L-mean} , a linear relationship was observed between the concentrations of NMHCs combined and R_{L-mean} , with a slope of 2.51 (Fig. 4a). A statistically significant correlation ($r = 0.599$, $n = 19$, $p = 0.007$) was observed when only plotting alkanes with R_{L-mean} . However, the correlation between alkenes and R_{L-mean} was statistically insignificant ($r = 0.248$, $n = 19$, $p = 0.306$).

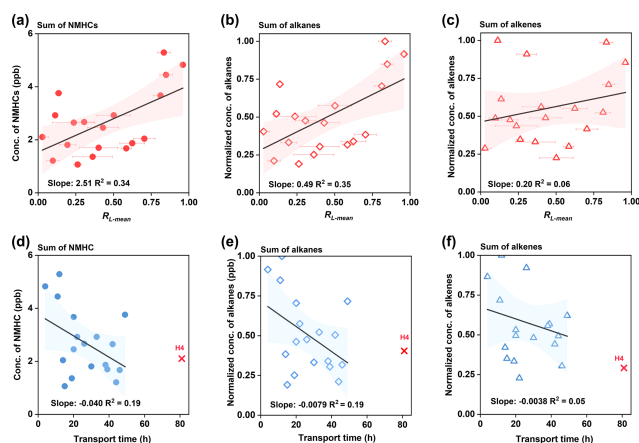


Figure 4. Concentrations of NMHCs combined (a, d), alkanes (b, e), and alkenes (c, f) at each site plotted against the mean retentions of air mass over land (R_{L-mean} , $n = 3$) and the transport time of air mass, respectively. The error bars for R_{L-mean} indicate the standard deviation from three different timescale trajectories (48, 72, and 96 h). The black line is the best fit of the liner function, and the shadowed area represents the confidence band at a 95 % confidence level. H4 (marked with red “x”) is treated as an outlier since it is the only value that deviates from the main dataset.

3.3.3 Transport time of air mass

The transport time of air mass was estimated as the interval from the last point of the trajectory contacting the continent to the moment when the air mass reached the sampling location, as detailed by Kato et al. (2001). These times ranged from 4 to 81 h, with an average of 30 h (Table S9). A shorter air mass transport time signifies a stronger terrestrial influence, as NMHCs within the air mass undergo further oxidation and dispersion over time. Total NMHC concentrations exhibited a significant decrease with an increase in air mass transport time, characterized by a slope of -0.04 (Fig. 4d). Alkanes displayed a steeper decline, indicated by a slope of -0.0079 (Fig. 4e), compared to alkenes (-0.0038 , Fig. 4f). Notably, elevated alkane concentrations were affected by air masses with larger R_{L-mean} (> 0.8) and shorter transport time (< 20 h) (Fig. S4). This emphasized the terrestrial influence on alkanes in the marine atmosphere since both R_L and transport time serve as indicators of air mass terrestrial characteristics. However, similar to the analysis of R_L , the correlation between the air mass transport time and alkenes was statistically insignificant ($r = 0.248$, $n = 19$, $p = 0.306$).

Overall, the analysis above suggests that the terrestrial input plays an important role in driving the variability observed for the atmospheric NMHCs over the marginal seas of China. In particular, a stronger terrestrial impact was determined for the alkanes based on the larger slopes from linear regression analysis and the significant correlations with terrestrial indicators. In contrast, no discernible trend was found for alkenes when plotting their concentrations against the distance from

sampling sites to the coastline (Fig. 2e, f). There was no significant correlation between alkenes and R_L or air mass transport time. Therefore, the variability of alkenes in the coastal atmosphere seems to be weakly impacted by the terrestrial sources when compared to alkanes. We attribute this to two main factors. First, the mean concentration of alkenes in the urban air was only 1.4 times higher than in the marine air, whereas it was 5.4 times higher for alkanes. Alkenes undergo more rapid oxidation due to their higher reactivities compared to alkanes during air mass transport. Secondly, oceanic ventilation may play a more substantial role in affecting marine alkenes (discussed in Sect. 3.4).

3.4 Oceanic impact on marine atmospheric NMHC composition

3.4.1 Sea-to-air fluxes of NMHCs

The mean (range) of sea-to-air fluxes of ethane, propane, i-butane, n-butane, ethylene, propylene, and isoprene was 44.6 ± 35.0 (0.2–118), 41.5 ± 39.9 (0.2–157), 31.7 ± 38.2 (0.1–146), 10.9 ± 25.4 (–0.8–96.1), 321 ± 294 (1.7–775), 56.1 ± 55.2 (0.2–212), and 112 ± 134 (0.5–468) $\text{nmol m}^{-2} \text{d}^{-1}$, respectively, in the Yellow Sea and the East China Sea (Table 1). These values were comparable to those reported in Chinese marginal seas (Wu et al., 2021; Li et al., 2021) and the 23–38° N Atlantic Ocean (Tran et al., 2013), but they were larger than the reported values in the North Sea (Broadgate et al., 1997) and the northwestern Pacific Ocean (Li et al., 2019; Wu et al., 2023) (Table S10).

The averaged sea-to-air fluxes of alkanes and alkenes within 100 km from the coastline were 147 ± 116 and 551 ± 497 $\text{nmol m}^{-2} \text{d}^{-1}$, respectively, which were relatively higher than those beyond 100 km (Fig. 5a, b). Since there were no significant differences in surface seawater temperature and 10 m wind speed between regions within and beyond 100 km from the coastline (Fig. S5), the discrepancy in fluxes might not be driven by physical processes. These elevated fluxes in the sea areas closer to land could be attributed to the influence of phytoplankton biomass and chromophoric dissolved organic matter (CDOM). Seawater NMHCs are not only directly synthesized by phytoplankton (Ratte et al., 1995), but they can also be emitted through the photochemical degradation of CDOM (Ratte et al., 1993; Lee and Baker, 1992). To substantiate our findings, we analyzed the monthly Chl-*a* concentration and the absorption coefficient at 443 nm of seawater in April 2021 from the remote sensing dataset from the NASA Ocean Color data service (NASA Ocean Biology Processing Group, 2022a, b) (Fig. S2). The mean (\pm SD) of Chl-*a* concentrations was 2.83 ± 1.17 and 1.68 ± 1.44 $\mu\text{g L}^{-1}$ in the areas within and beyond 100 km from the coastline, respectively. Correspondingly, the mean (\pm SD) of seawater absorption coefficients at 443 nm was 0.124 ± 0.060 and 0.069 ± 0.040 m^{-1} , respectively. Hence, the heightened phytoplankton biomass and enriched pho-

to-reaction substrate collectively enhanced both the biological production of NMHCs and the abiotic formation of NMHCs, consequently resulting in a pronounced NMHC emission in nearshore regions.

3.4.2 Assessing the effect of oceanic emission on NMHCs

Prior to delving into the correlation between oceanic emissions and NMHC concentrations, it is imperative to acknowledge the influence of different gases' reactivity on this relationship. For instance, ethane possesses an atmospheric lifetime of approximately 78 d at 24 h [$\cdot\text{OH}$] concentration of 6×10^5 molec. cm^{-3} (Jobson et al., 1999), using the rate constant with $\cdot\text{OH}$ at 288 K taken from Atkinson et al. (1997). The relatively long atmospheric residence time of ethane facilitates its accumulation in the atmosphere. Conversely, isoprene, with a much shorter lifetime of only 0.2 d, emitted within a very brief window can impact its atmospheric level. Thus, to mitigate the impact of varying reactivity among the different gas species, we calculated the lifetime-weighted concentrations of each NMHC according to its atmospheric lifetime (introduced in Sect. 2.5). This novel method is more nuanced in assessing the impact of oceanic emission on atmospheric NMHCs, as it acknowledges not only their abundance but also their residence in the atmosphere.

Despite the elevated oceanic emission of NMHCs within 100 km from land, its impact on atmospheric NMHC composition was comparatively weak, displaying a slope of 0.0187 (Fig. 5c), which was lower than the fitted result of the dataset in areas beyond 100 km from land with a slope of 0.0415 (Fig. 5d). This could be attributed to the disturbance of terrestrial outflow in nearshore areas, mitigating the direct impact of oceanic emission on NMHCs. As it extended further from land, the terrestrial influence diminished. This, in turn, strengthens the regulatory impact of oceanic emission on atmospheric NMHC levels.

In addition, the average flux of total alkenes across the entire region was 163 ± 221 $\text{nmol m}^{-2} \text{d}^{-1}$, which was approximately 5 times higher than that of alkanes (32.2 ± 37.5 $\text{nmol m}^{-2} \text{d}^{-1}$). This substantial discrepancy indicates that alkanes and alkenes are certainly influenced differently by oceanic emissions. The correlation between the lifetime-weighted concentrations of alkenes and their fluxes was statistically significant ($r = 0.548$, $n = 57$, $p < 0.001$), while it was insignificant for alkanes ($r = 0.113$, $n = 76$, $p = 0.329$). When specific species of alkanes (Fig. 5e) and alkenes (Fig. 5f) were separately plotted against their sea-to-air fluxes, alkenes exhibited a steeper slope of 0.0072 compared to the slope of 0.0044 for alkanes. This signifies that oceanic emission has a more significant impact on atmospheric alkenes compared to alkanes, which verifies our hypothesis as stated at the end of Sect. 3.3.

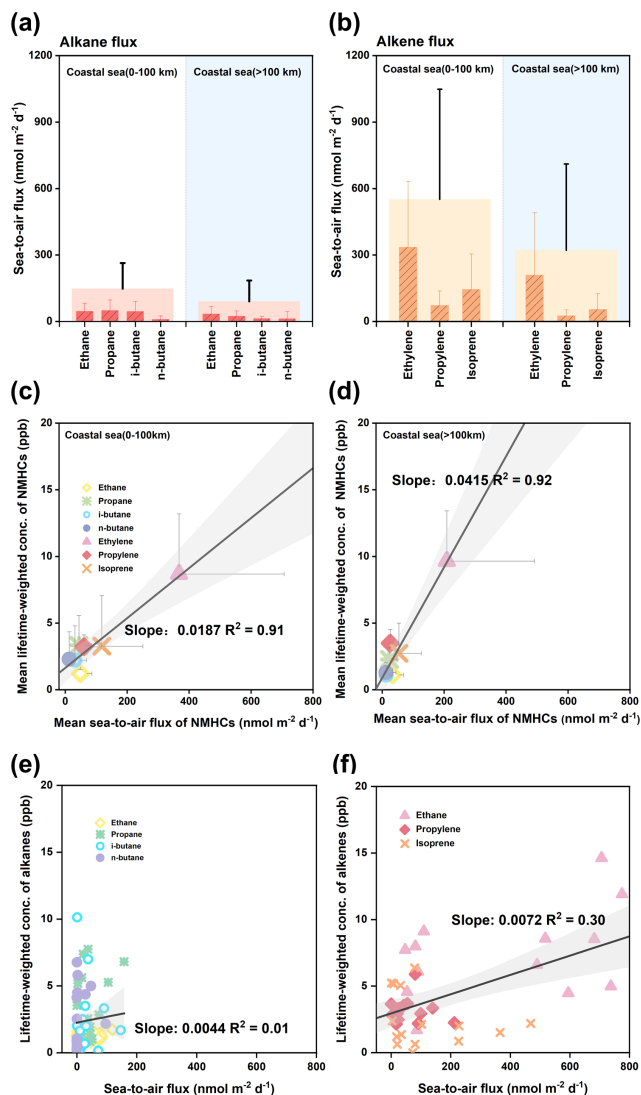


Figure 5. Means of sea-to-air fluxes of alkanes (a) and alkenes (b) in sea areas within 100 km ($n = 10$) and beyond 100 km ($n = 9$) from the nearshore land. The wider columns represent the sum of alkanes and alkenes. Panels (c) and (d) show the means of lifetime-weighted concentrations of NMHCs plotted against their mean sea-to-air fluxes in the area within 100 km or beyond 100 km from the coastline. Specific lifetime-weighted concentrations of alkanes (e) and alkenes (f) plotted against sea-to-air fluxes in the whole coastal sea region. The black lines are the best linear fit for each dataset, and the shadowed area represents the confidence band at a 95 % confidence level.

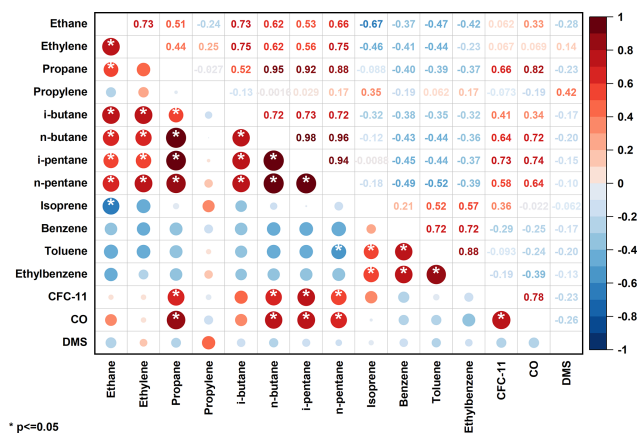


Figure 6. Correlation coefficients (r) between the various trace gases determined in the atmosphere over the Yellow Sea and the East China Sea. The white asterisk means the correlation is significant at $p < 0.05$. The color of the dots, red and blue, indicates the positive and negative correlation, and the size of the dots indicates the absolute value of r .

3.5 Identification and apportionment of the sources of marine atmospheric NMHCs

3.5.1 Source identification

Since the chemical compositions are largely controlled by the sources of emissions, specific ratios of hydrocarbons have been widely employed to identify the sources of NMHCs (Gilman et al., 2013; Rossabi and Helmig, 2018). For instance, elevated isopentane/*n*-pentane ratios are indicative of the large influence of vehicular emissions (2.2–3.8) and gasoline fuel evaporation (1.8–4.6) (Gentner et al., 2009; Jobson et al., 2004; Liu et al., 2008; Russo et al., 2010). Conversely, the lower ratios indicate the importance of tropical forest fires (0.43–0.57) (Andreae and Merlet, 2001; Rossabi and Helmig, 2018), natural and oil gas operations (0.81–1.1) (Gilman et al., 2013; Swarthout et al., 2013), and marine vessel exhaust (1.59–1.71) (Bourtsoukidis et al., 2019) in controlling the chemical composition of NMHCs. In this study, a significant correlation was observed between *i*-pentane and *n*-pentane ($r = 0.67$, $p < 0.01$) (Fig. 6), and the *i*-pentane/*n*-pentane ratio spans a wider range from 0.89 to 2.46, suggesting that the composition of NMHCs in the marginal seas of China is controlled by multiple sources, e.g., natural and oil gas operations, marine vessel exhaust, vehicular emissions, and gasoline evaporation.

Furthermore, propane, *i*-butane, and *n*-butane exhibited strong intercorrelations ($r = 0.52$ – 0.95 , $p < 0.05$). They also displayed strong correlations with ethane, *i*-pentane, and *n*-pentane ($r = 0.55$ – 0.98 , $p < 0.05$). These alkanes have been recognized as the primary components of liquid petroleum gases (Blake and Rowland, 1995), extensively utilized as fuel in taxis, private cars, and public buses in China (Guo et al., 2017; Zhang et al., 2015). Notably, C3–C5 alkanes also ex-

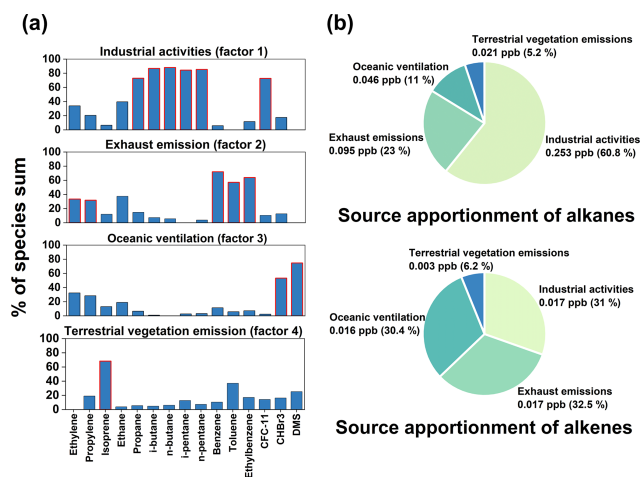


Figure 7. Representative factor profiles from the PMF model (a) and relative contributions of different factors/sources to the alkanes and alkenes in the oceanic atmosphere (b). NMHCs in panel a marked with red rim are selected as indicators for the specific factors.

hibited significant correlations with ethane ($r = 0.55\text{--}0.72$, $p < 0.05$) and carbon monoxide ($r = 0.59\text{--}0.81$, $p < 0.05$), while ethane and carbon monoxide are acknowledged tracers of fossil fuel or biomass/biofuel combustion and incomplete combustion, respectively (Lai et al., 2010; Tang et al., 2009; Parrish et al., 2009). This indicated the contribution of vehicular emissions of liquid petroleum gases and combustion of fossil fuel or biomass to light alkanes. Additionally, strong correlations were observed among monocyclic aromatics (benzene, toluene, ethylbenzene) ($r = 0.67\text{--}0.83$, $p < 0.05$). This finding was consistent with recent emission inventory research identifying monocyclic aromatics as significant constituents of ship exhaust (Xiao et al., 2018b; Wu et al., 2019). As for oceanic emissions, we present the sea-to-air fluxes of NMHCs and discuss the significant effect of oceanic emissions on NMHCs in Sect. 3.4. Multiple studies have highlighted that the ocean is one of the most important sources of these gases (Kato et al., 2007; Li et al., 2019; Mallik et al., 2013; Sahu et al., 2010; Rudolph and Johnen, 1990).

3.5.2 Source apportionment

The potential sources of atmospheric NMHCs and their respective contributions to each category were determined using the PMF model. Four isolate factors were extracted according to their composition profiles depicted in Fig. 7a. These factors, including industrial production, exhaust emission, terrestrial vegetation, and oceanic ventilation, were identified based on chemical profiles in the literature.

Propane, i-butane, n-butane, i-pentane, n-pentane, and CFC-11 showed strong loadings ($> 70\%$) on factor 1. The presence of propane, butanes, and pentanes suggests an in-

fluence of refinery activities (Buzcu and Fraser, 2006). Additionally, propane has been recognized as a characteristic NMHC derived from natural gas emissions, and butane is indicative of liquefied petroleum gas (LPG) (Guo et al., 2011; Tsai et al., 2006; Hui et al., 2018; Ho et al., 2009). Moreover, CFC-11 is a typical artificial industrial product. Subsequently, factor 1 was identified as a factor relating to industrial activities.

The profile of factor 2 showed strong loadings of benzene (72%), toluene (57%), and ethylbenzene (64%), along with moderate impacts of ethylene (34%) and propylene (32%). Benzene emissions are notably associated with vehicle exhaust (Zhang et al., 2013, 2016), and considerable fractions of aromatics can be emitted from ship exhaust during both berthing and cruising (Cooper, 2005; Xiao et al., 2018a). C₂–C₄ alkenes could stem from ship emissions in the open ocean (Eyring et al., 2005). Therefore, factor 2 can be assigned as a potential source of exhaust emissions of vehicles and ships.

Factor 3 was assigned as oceanic ventilation due to elevated percentages of DMS (74%) and CHBr₃ (53%), considering the dominant contributions of ocean emission to DMS (Lana et al., 2011; Lee and Brimblecombe, 2016) and CHBr₃ (Quack and Wallace, 2003; Ashfold et al., 2014). Factor 4 was mainly characterized by a high percentage of isoprene (68%), an indicator of biogenic emission from terrestrial vegetation (Guenther et al., 2006; Wu et al., 2016). However, given isoprene's high reactivity, this factor should be treated cautiously and regarded as a lower limit (Fujita, 2001). Although its short atmospheric lifetime hinders long-range transport, the minimum air mass transport time from land to the oceanic station was 4 h in this study, implying the potential for terrestrial isoprene to reach the nearshore atmosphere.

According to the results of the PMF model analysis, the dominant source of atmospheric alkanes in the Chinese marginal seas was industrial activities (0.253 ppb, 60.8%), followed by exhaust emissions (0.095 ppb, 23%). Contributions from terrestrial vegetation emission (0.049 ppb, 11%) and oceanic ventilation (0.021 ppb, 5.2%) were relatively smaller. Furthermore, exhaust emissions (0.017 ppb, 32.5%), industrial activities (0.017 ppb, 31%), and ocean ventilation (0.016 ppb, 30.4%) contribute almost equally to atmospheric alkenes. Collectively, these three factors constitute the main sources of alkenes (93.8%), whereas the contribution from terrestrial vegetation is minimal, at merely 6.2%. Particularly, the contribution of terrestrial sources to alkanes (89%) is greater than that to alkenes (69.6%), while the contribution of ocean emission to alkenes (30.4%) is greater than that to alkanes (5.2%). This is consistent with the conclusions in Sect. 3.3 and 3.4.

It must be acknowledged that the classification and quantification results derived from the PMF model inevitably involve uncertainties that are challenging to ascertain precisely. These uncertainties are primarily attributed to factors such as the number of gas species, the number of samples, and the

temporal and spatial resolutions of sampling. However, it is noteworthy that the PMF analysis results are relatively consistent with the phenomena described in Sect. 3.3 and 3.4. This consistency to some extent validates the accuracy of the PMF analysis and underscores the significant contribution and impact of terrestrial inputs on the atmospheric NMHCs in the marginal seas of China.

3.5.3 Contributions of terrestrial/oceanic NMHCs to SOA and ozone

P_{SOAP} of the C2–C5 NMHCs in the atmosphere over the Chinese marginal seas was $0.41 \pm 0.18 \mu\text{g m}^{-3}$, with terrestrial sources contributing the majority ($0.32 \pm 0.14 \mu\text{g m}^{-3}$), accounting for approximately 78 % (Fig. 8a). Specifically, P_{SOAP} from terrestrial alkanes and alkenes was 0.17 ± 0.07 and $0.15 \pm 0.06 \mu\text{g m}^{-3}$, respectively, while marine sources contributed 0.02 ± 0.01 and $0.07 \pm 0.03 \mu\text{g m}^{-3}$ for alkanes and alkenes, respectively. Additionally, troposphere aerosol concentrations over the Chinese marginal seas during the investigation period were calculated using data from the NASA Goddard Earth Sciences Data and Information Services Center (GES DISC), ranging from 0.77 to $3.98 \mu\text{g m}^{-3}$, with an average of $1.80 \pm 0.71 \mu\text{g m}^{-3}$. The aerosol concentrations decreased from the coastal areas towards the open sea (Fig. 8b), suggesting an obvious influence of terrestrial inputs on the aerosol levels in the coastal atmosphere. Based on the remote sensing data, it is roughly estimated that terrestrial C2–C5 NMHCs contribute $\sim 18\%$ to the total aerosol concentration, indicating their non-negligible role in influencing the atmospheric aerosol levels over the marginal seas.

Similarly, the OFF of alkanes and alkenes from terrestrial sources was 2.35 ± 1.01 and $1.18 \pm 0.51 \mu\text{g m}^{-3}$, respectively, significantly higher than that from marine sources ($0.14 \pm 0.06 \mu\text{g m}^{-3}$ for alkanes and $0.50 \pm 0.21 \mu\text{g m}^{-3}$ for alkenes) (Fig. 8c). However, the ozone distribution in the offshore atmosphere of China showed a decreasing trend from north to south (Fig. 8d). The marine atmosphere generally acts as a net ozone sink with ozone being primarily removed by photochemical degradation (Monks et al., 1998; Conley et al., 2011). The increasing solar radiation intensity from north to south enhances ozone degradation rates, likely dominating the ozone distribution in China's offshore atmosphere. Notably, satellite observations (GES DISC) during this investigation period indicated that the tropospheric ozone was approximately $82.6 \pm 3.08 \mu\text{g m}^{-3}$ over the Chinese marginal seas. Among this, terrestrial C2–C5 NMHCs contributed around 4 % to total ozone concentration, suggesting a certain impact of terrestrial outflow on the tropospheric ozone in these regions.

4 Conclusions

Our study characterized the atmospheric NMHCs in both coastal cities and Chinese marginal seas and determined that

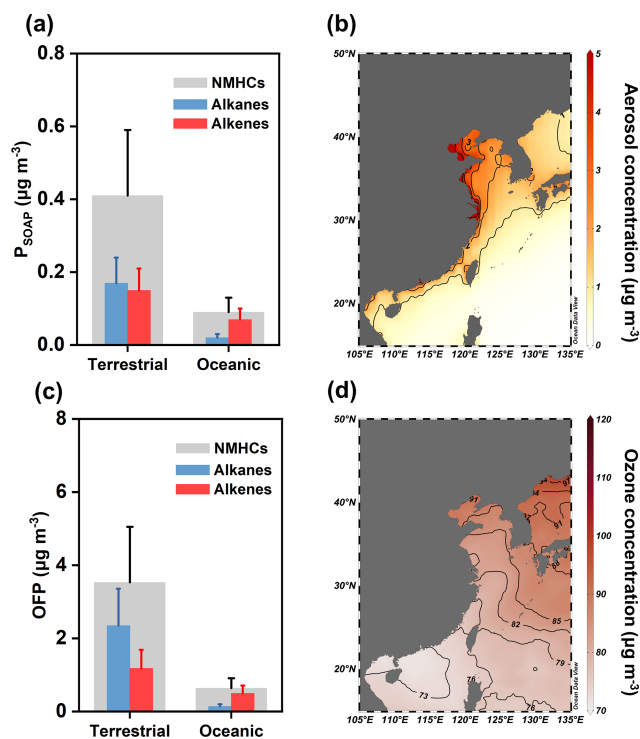


Figure 8. P_{SOAP} (a) and OFF (c) of NMHCs and averaged concentration of troposphere aerosol (b) and ozone (d) during the investigation period over the Chinese marginal seas. Data of aerosol (Global Modeling and Assimilation Office and Pawson, 2015) and ozone (Miyazaki, 2024) were downloaded from GES DISC (Schlitzer, 2023).

both oceanic ventilation and terrestrial inputs play important roles in controlling the distribution and chemical composition of NMHCs in the coastal atmosphere of China.

Alkanes were the dominant NMHCs in both urban and nearshore atmospheres, and the atmospheric concentrations of alkanes were significantly higher in coastal cities compared to coastal seas, showing the potential of terrestrial alkanes as a source of alkanes in the marine atmosphere through transport. Generally, alkane concentrations tended to be higher in cases where the sampling sites were closer to land, there was a longer retention of air mass over land, and there was a shorter air mass transport time from land to the sampling site. However, these effects could not apply to alkenes due to their higher reactivities and the substantial sea-to-air fluxes. Additionally, the impact of oceanic emissions on NMHC composition was more pronounced in areas beyond 100 km from land compared to areas within 100 km because the terrestrial input gradually diminishes along the direction towards the open ocean.

Combining the outcomes of the PMF model and chemical profiles of diverse sources in the literature, we extracted four isolated sources of NMHCs in the nearshore atmosphere. Terrestrial sources (including industrial activities, vehicular exhaust, and vegetation emission) primarily consti-

tute the NMHCs in the nearshore atmospheres, and they partially influence atmospheric SOA and ozone levels. This indicates the potential importance of terrestrial outflow in shaping the air quality and regulating climate dynamics in the marginal seas.

Code and data availability. Data presented in this paper are publicly available on Figshare via <https://doi.org/10.6084/m9.figshare.24722286.v1> (Wang, 2023). The remote sensing datasets of Chl *a* and total absorption at 443 nm are available at <https://doi.org/10.5067/AQUA/MODIS/L3M/CHL/2022> (NASA Ocean Biology Processing Group, 2022a) and <https://doi.org/10.5067/AQUA/MODIS/L3M/IOP/2022> (NASA Ocean Biology Processing Group, 2022b), respectively. The datasets of aerosol and ozone are available at <https://doi.org/10.5067/6QS7DO2FZVY1> (Miyazaki, 2024) and <https://doi.org/10.5067/QBZ6MG944HW0> (Global Modeling and Assimilation Office and Pawson, 2015), respectively. Code to calculate the retention of air mass over land can be downloaded from <https://doi.org/10.6084/m9.figshare.26499985> (Wang, 2024).

Supplement. The supplement related to this article is available online at: <https://doi.org/10.5194/acp-24-8721-2024-supplement>.

Author contributions. HZ and JW designed the investigation and experiments. JW, QM, FX, GX, SY, JZ, and JL collected and determined the samples. JW analyzed the data and wrote the paper. HZ, LX, ZC, and GZ reviewed and revised the paper.

Competing interests. The contact author has declared that none of the authors has any competing interests.

Disclaimer. Publisher's note: Copernicus Publications remains neutral with regard to jurisdictional claims made in the text, published maps, institutional affiliations, or any other geographical representation in this paper. While Copernicus Publications makes every effort to include appropriate place names, the final responsibility lies with the authors.

Acknowledgements. We thank the chief scientist, captain, and crew of the R/V *Dong Fang Hong 3* for their assistance and cooperation during the investigation. We would like to acknowledge the NOAA Air Resources Laboratory for the provision of the HYSPLIT trajectory model used in this study and the NASA Ocean Color data service for the provision of the remote sensing dataset of Chl *a* and total absorption at 443 nm in this study region.

Financial support. This work was financially supported by the National Natural Science Foundation of China (grant nos. 42276042, 41876082, 42225601, and 42006044), the Laoshan Laboratory (grant no. LSKJ 202201701), and the Fundamental Re-

search Funds for the Central Universities (grant nos. 202372001 and 202072001).

Review statement. This paper was edited by John Liggio and reviewed by three anonymous referees.

References

- Andreae, M. O. and Merlet, P.: Emission of trace gases and aerosols from biomass burning, *Glob. Biogeochem. Cycle*, 15, 955–966, <https://doi.org/10.1029/2000GB001382>, 2001.
- Ashfold, M. J., Harris, N. R. P., Manning, A. J., Robinson, A. D., Warwick, N. J., and Pyle, J. A.: Estimates of tropical bromoform emissions using an inversion method, *Atmos. Chem. Phys.*, 14, 979–994, <https://doi.org/10.5194/acp-14-979-2014>, 2014.
- Atkinson, R., Baulch, D. L., Cox, R. A., Hampson, R. F., Kerr, J. A., Rossi, M. J., and Troe, J.: Evaluated kinetic, photochemical and heterogeneous data for atmospheric chemistry .5. Iupac subcommittee on gas kinetic data evaluation for atmospheric chemistry, *J. Phys. Chem. Ref. Data*, 26, 521–1011, <https://doi.org/10.1063/1.556011>, 1997.
- Blake, D. R. and Rowland, F. S.: Urban leakage of liquefied petroleum gas and its impact on Mexico City air quality, *Science*, 269, 953–956, <https://doi.org/10.1126/science.269.5226.953>, 1995.
- Bonsang, B., Polle, C., and Lambert, G.: Evidence for marine production of isoprene, *Geophys. Res. Lett.*, 19, 1129–1132, <https://doi.org/10.1029/92GL00083>, 1992.
- Bourtsoukidis, E., Ernle, L., Crowley, J. N., Lelieveld, J., Paris, J.-D., Pozzer, A., Walter, D., and Williams, J.: Non-methane hydrocarbon (C₂–C₈) sources and sinks around the Arabian Peninsula, *Atmos. Chem. Phys.*, 19, 7209–7232, <https://doi.org/10.5194/acp-19-7209-2019>, 2019.
- Broadgate, W. J., Liss, P. S., and Penkett, S. A.: Seasonal emissions of isoprene and other reactive hydrocarbon gases from the ocean, *Geophys. Res. Lett.*, 24, 2675–2678, <https://doi.org/10.1029/97GL02736>, 1997.
- Buzcu, B. and Fraser, M. P.: Source identification and apportionment of volatile organic compounds in Houston, TX, *Atmos. Environ.*, 40, 2385–2400, <https://doi.org/10.1016/j.atmosenv.2005.12.020>, 2006.
- Carter, W. P. L.: Development of a condensed SAPRC-07 chemical mechanism, *Atmos. Environ.*, 44, 5336–5345, <https://doi.org/10.1016/j.atmosenv.2010.01.024>, 2010.
- Carter, W. P. L.: Development of ozone reactivity scales for volatile organic compounds, *J. Air Waste Manag. Assoc.*, 44, 881–899, <https://doi.org/10.1080/1073161X.1994.10467290>, 1994.
- Conley, S. A., Faloona, I. C., Lenschow, D. H., Campos, T., Heizer, C., Weinheimer, A., Cantrell, C. A., Mauldin, R. L., Hornbrook, R. S., Pollack, I., and Bandy, A.: A complete dynamical ozone budget measured in the tropical marine boundary layer during PASE, *J. Atmos. Chem.*, 66, 55–70, <https://doi.org/10.1007/s10874-011-9195-0>, 2011.
- Cooper, D. A.: Hcb, pcb, pcd and pcd emissions from ships, *Atmos. Environ.*, 39, 4901–4912, <https://doi.org/10.1016/j.atmosenv.2005.04.037>, 2005.

- Decesari, S., Paglione, M., Rinaldi, M., Dall'Osto, M., Simó, R., Zanca, N., Volpi, F., Facchini, M. C., Hoffmann, T., Götz, S., Kampf, C. J., O'Dowd, C., Ceburnis, D., Ovadnevaite, J., and Tagliavini, E.: Shipborne measurements of Antarctic sub-micron organic aerosols: an NMR perspective linking multiple sources and bioregions, *Atmos. Chem. Phys.*, 20, 4193–4207, <https://doi.org/10.5194/acp-20-4193-2020>, 2020.
- Ding, A., Wang, T., Zhao, M., Wang, T., and Li, Z. K.: Simulation of sea-land breezes and a discussion of their implications on the transport of air pollution during a multi-day ozone episode in the Pearl River Delta of China, *Atmos. Environ.*, 38, 6737–6750, <https://doi.org/10.1016/j.atmosenv.2004.09.017>, 2004.
- Eyring, V., Kohler, H. W., van Aardenne, J., and Lauer, A.: Emissions from international shipping: 1. The last 50 years, *J. Geophys. Res.-Atmos.*, 110, D17305, <https://doi.org/10.1029/2004JD005619>, 2005.
- Fujita, E. M.: Hydrocarbon source apportionment for the 1996 Paso del Norte Ozone Study, *Sci. Total Environ.*, 276, 171–184, [https://doi.org/10.1016/S0048-9697\(01\)00778-1](https://doi.org/10.1016/S0048-9697(01)00778-1), 2001.
- Gentner, D. R., Harley, R. A., Miller, A. M., and Goldstein, A. H.: Diurnal and seasonal variability of gasoline-related volatile organic compound emissions in riverside, California, *Environ. Sci. Technol.*, 43, 4247–4252, <https://doi.org/10.1021/es9006228>, 2009.
- Gilman, J. B., Lerner, B. M., Kuster, W. C., and de Gouw, J. A.: Source signature of volatile organic compounds from oil and natural gas operations in Northeastern Colorado (vol 47, pg 1297, 2013), *Environ. Sci. Technol.*, 47, 10094–10094, <https://doi.org/10.1021/es4036978>, 2013.
- Global Modeling and Assimilation Office and Pawson, S.: MERRA-2 inst3_3d_asm_Np: 3d, 3-Hourly, Instantaneous, Pressure-Level, Assimilation, Assimilated Meteorological Fields V5.12.4, NASA Goddard Earth Sciences Data and Information Services Center [data set], <https://doi.org/10.5067/QBZ6MG944HW0>, 2015.
- Grosjean, D. and Seinfeld, J. H.: Parameterization of the formation potential of secondary organic aerosols. *Atmos. Environ.* 23, 1733–1747, [https://doi.org/10.1016/0004-6981\(89\)90058-9](https://doi.org/10.1016/0004-6981(89)90058-9), 1989.
- Guenther, A., Karl, T., Harley, P., Wiedinmyer, C., Palmer, P. I., and Geron, C.: Estimates of global terrestrial isoprene emissions using MEGAN (Model of Emissions of Gases and Aerosols from Nature), *Atmos. Chem. Phys.*, 6, 3181–3210, <https://doi.org/10.5194/acp-6-3181-2006>, 2006.
- Guenther, A., Hewitt, C. N., Erickson, D., Fall, R., Geron, C., Graedel, T., Harley, P., Klinger, L., Lerdau, M., McKay, W. A., Pierce, T., Scholes, B., Steinbrecher, R., Tallamraju, R., Taylor, J., and Zimmerman, P.: A global-model of natural volatile organic-compound emissions, *J. Geophys. Res.-Atmos.*, 100, 8873–8892, <https://doi.org/10.1029/94JD02950>, 1995.
- Guenther, A. B., Jiang, X., Heald, C. L., Sakulyanontvittaya, T., Duhl, T., Emmons, L. K., and Wang, X.: The Model of Emissions of Gases and Aerosols from Nature version 2.1 (MEGAN2.1): an extended and updated framework for modeling biogenic emissions, *Geosci. Model Dev.*, 5, 1471–1492, <https://doi.org/10.5194/gmd-5-1471-2012>, 2012.
- Guo, H., Cheng, H. R., Ling, Z. H., Louie, P. K. K., and Ayoko, G. A.: Which emission sources are responsible for the volatile organic compounds in the atmosphere of Pearl River Delta?, *J. Hazard. Mater.*, 188, 116–124, <https://doi.org/10.1016/j.jhazmat.2011.01.081>, 2011.
- Guo, H., Ling, Z. H., Cheng, H. R., Simpson, I. J., Lyu, X. P., Wang, X. M., Shao, M., Lu, H. X., Ayoko, G., Zhang, Y. L., Saunders, S. M., Lam, S. H. M., Wang, J. L., and Blake, D. R.: Tropospheric volatile organic compounds in China, *Sci. Total Environ.*, 574, 1021–1043, <https://doi.org/10.1016/j.scitotenv.2016.09.116>, 2017.
- Hallquist, M., Wenger, J. C., Baltensperger, U., Rudich, Y., Simpson, D., Claeys, M., Dommen, J., Donahue, N. M., George, C., Goldstein, A. H., Hamilton, J. F., Herrmann, H., Hoffmann, T., Iinuma, Y., Jang, M., Jenkin, M. E., Jimenez, J. L., Kiendler-Scharr, A., Maenhaut, W., McFiggans, G., Mentel, Th. F., Monod, A., Prévôt, A. S. H., Seinfeld, J. H., Surratt, J. D., Szmigielski, R., and Wildt, J.: The formation, properties and impact of secondary organic aerosol: current and emerging issues, *Atmos. Chem. Phys.*, 9, 5155–5236, <https://doi.org/10.5194/acp-9-5155-2009>, 2009.
- He, Z., Wang, X., Ling, Z., Zhao, J., Guo, H., Shao, M., and Wang, Z.: Contributions of different anthropogenic volatile organic compound sources to ozone formation at a receptor site in the Pearl River Delta region and its policy implications, *Atmos. Chem. Phys.*, 19, 8801–8816, <https://doi.org/10.5194/acp-19-8801-2019>, 2019.
- Ho, K. F., Lee, S. C., Ho, W. K., Blake, D. R., Cheng, Y., Li, Y. S., Ho, S. S. H., Fung, K., Louie, P. K. K., and Park, D.: Vehicular emission of volatile organic compounds (VOCs) from a tunnel study in Hong Kong, *Atmos. Chem. Phys.*, 9, 7491–7504, <https://doi.org/10.5194/acp-9-7491-2009>, 2009.
- Houweling, S., Dentener, F., and Lelieveld, J.: The impact of nonmethane hydrocarbon compounds on tropospheric photochemistry, *J. Geophys. Res.-Atmos.*, 103, 10673–10696, <https://doi.org/10.1029/97JD03582>, 1998.
- Hui, L., Liu, X., Tan, Q., Feng, M., An, J., Qu, Y., Zhang, Y., and Jiang, M.: Characteristics, source apportionment and contribution of vocs to ozone formation in Wuhan, Central China, *Atmos. Environ.*, 192, 55–71, <https://doi.org/10.1016/j.atmosenv.2018.08.042>, 2018.
- Jobson, B. T., McKeen, S. A., Parrish, D. D., Fehsenfeld, F. C., Blake, D. R., Goldstein, A. H., Schauffler, S. M., and Elkins, J. C.: Trace gas mixing ratio variability versus lifetime in the troposphere and stratosphere: Observations, *J. Geophys. Res.-Atmos.*, 104, 16091–16113, <https://doi.org/10.1029/1999JD900126>, 1999.
- Jobson, B. T., Parrish, D. D., Goldan, P., Kuster, W., Fehsenfeld, F. C., Blake, D. R., Blake, N. J., and Niki, H.: Spatial and temporal variability of nonmethane hydrocarbon mixing ratios and their relation to photochemical lifetime, *J. Geophys. Res.-Atmos.*, 103, 13557–13567, <https://doi.org/10.1029/97JD01715>, 1998.
- Jobson, B. T., Berkowitz, C. M., Kuster, W. C., Goldan, P. D., Williams, E. J., Fehsenfeld, F. C., Apel, E. C., Karl, T., Lonneman, W. A., and Riemer, D.: Hydrocarbon source signatures in Houston, Texas: Influence of the petrochemical industry, *J. Geophys. Res.-Atmos.*, 109, D24305, <https://doi.org/10.1029/2004JD004887>, 2004.
- Kato, S., Pochanart, P., and Kajii, Y.: Measurements of ozone and nonmethane hydrocarbons at Chichi-jima island, a remote island in the Western Pacific: Long-range transport of polluted air

- from the Pacific rim region, *Atmos. Environ.*, 35, 6021–6029, [https://doi.org/10.1016/S1352-2310\(01\)00453-8](https://doi.org/10.1016/S1352-2310(01)00453-8), 2001.
- Kato, S., Ui, T., Uematsu, M., and Kajii, Y.: Trace gas measurements over the Northwest Pacific during the 2002 IOC cruise, *Geochem. Geophys. Geosyst.*, 8, Q06M10, <https://doi.org/10.1029/2006GC001241>, 2007.
- Kato, S., Kajii, Y., Itokazu, R., Hirokawa, J., Koda, S., and Kinjo, Y.: Transport of atmospheric carbon monoxide, ozone, and hydrocarbons from Chinese coast to Okinawa island in the Western Pacific during winter, *Atmos. Environ.*, 38, 2975–2981, <https://doi.org/10.1016/j.atmosenv.2004.02.049>, 2004.
- Lai, S. C., Baker, A. K., Schuck, T. J., van Velthoven, P., Oram, D. E., Zahn, A., Hermann, M., Weigelt, A., Slemr, F., Breninkmeijer, C. A. M., and Ziereis, H.: Pollution events observed during CARIBIC flights in the upper troposphere between South China and the Philippines, *Atmos. Chem. Phys.*, 10, 1649–1660, <https://doi.org/10.5194/acp-10-1649-2010>, 2010.
- Lana, A., Bell, T. G., Simo, R., Vallina, S. M., Ballabrera-Poy, J., Kettle, A. J., Dachs, J., Bopp, L., Saltzman, E. S., Stefels, J., Johnson, J. E., and Liss, P. S.: An updated climatology of surface dimethylsulfide concentrations and emission fluxes in the global ocean, *Glob. Biogeochem. Cycle*, 25, GB1004, <https://doi.org/10.1029/2010GB003850>, 2011.
- Lee, C. L. and Brimblecombe, P.: Anthropogenic contributions to global carbonyl sulfide, carbon disulfide and organosulfides fluxes, *Earth-Sci. Rev.*, 160, 1–18, <https://doi.org/10.1016/j.earscirev.2016.06.005>, 2016.
- Lee, R. F. and Baker, J.: Ethylene and ethane production in an estuarine river: Formation from the decomposition of polyunsaturated fatty acids, *Mar. Chem.*, 38, 25–36, [https://doi.org/10.1016/0304-4203\(92\)90065-I](https://doi.org/10.1016/0304-4203(92)90065-I), 1992.
- Li, J. L., Zhai, X., Ma, Z., Zhang, H. H., and Yang, G. P.: Spatial distributions and sea-to-air fluxes of non-methane hydrocarbons in the atmosphere and seawater of the Western Pacific Ocean, *Sci. Total Environ.*, 672, 491–501, <https://doi.org/10.1016/j.scitotenv.2019.04.019>, 2019.
- Li, J. L., Zhai, X., Wu, Y. C., Wang, J., Zhang, H. H., and Yang, G. P.: Emissions and potential controls of light alkenes from the marginal seas of China, *Sci. Total Environ.*, 758, 143655, <https://doi.org/10.1016/j.scitotenv.2020.143655>, 2021.
- Li, L. Y., Xie, S. D., Zeng, L. M., Wu, R. R., and Li, J.: Characteristics of volatile organic compounds and their role in ground-level ozone formation in the Beijing-Tianjin-Hebei region, China, *Atmos. Environ.*, 113, 247–254, <https://doi.org/10.1016/j.atmosenv.2015.05.021>, 2015.
- Liu, B. S., Liang, D. N., Yang, J. M., Dai, Q. L., Bi, X. H., Feng, Y. C., Yuan, J., Xiao, Z. M., Zhang, Y. F., and Xu, H.: Characterization and source apportionment of volatile organic compounds based on 1-year of observational data in Tianjin, China, *Environ. Pollut.*, 218, 757–769, <https://doi.org/10.1016/j.envpol.2016.07.072>, 2016.
- Liu, Y., Shao, M., Fu, L., Lu, S., Zeng, L., and Tang, D.: Source profiles of volatile organic compounds (VOCs) measured in China: Part i, *Atmos. Environ.*, 42, 6247–6260, <https://doi.org/10.1016/j.atmosenv.2008.01.070>, 2008.
- Mallik, C., Lal, S., Venkataramani, S., Naja, M., and Ojha, N.: Variability in ozone and its precursors over the bay of Bengal during post monsoon: Transport and emission effects, *J. Geophys. Res.-Atmos.*, 118, 10190–10209, <https://doi.org/10.1002/jgrd.50764>, 2013.
- Messina, P., Lathière, J., Sindelarova, K., Vuichard, N., Granier, C., Ghattas, J., Cozic, A., and Hauglustaine, D. A.: Global biogenic volatile organic compound emissions in the ORCHIDEE and MEGAN models and sensitivity to key parameters, *Atmos. Chem. Phys.*, 16, 14169–14202, <https://doi.org/10.5194/acp-16-14169-2016>, 2016.
- Miyazaki, K.: TROPES Chemical Reanalysis Surface Aerosol NH₄ 2-Hourly 2-dimensional Product, NASA Goddard Earth Sciences Data and Information Services Center [data set], <https://doi.org/10.5067/6QS7DO2FZVY1>, 2024.
- Monks, P. S., Carpenter, L. J., Penkett, S. A., Ayers, G. P., Gillett, R. W., Galbally, I. E., and Meyer, C. P.: Fundamental ozone photochemistry in the remote marine boundary layer: the soapex experiment, measurement and theory, *Atmos. Environ.*, 32, 3647–3664, [https://doi.org/10.1016/S1352-2310\(98\)00084-3](https://doi.org/10.1016/S1352-2310(98)00084-3), 1998.
- NASA Ocean Biology Processing Group: Aqua MODIS Level 3 Mapped Chlorophyll Data, Version R2022.0, NASA Ocean Biology Distributed Active Archive Center [data set], <https://doi.org/10.5067/AQUA/MODIS/L3M/CHL/2022>, 2022a.
- NASA Ocean Biology Processing Group: Aqua MODIS Level 3 Mapped Inherent Optical Properties Data, Version R2022.0, NASA Ocean Biology Distributed Active Archive Center [data set], <https://doi.org/10.5067/AQUA/MODIS/L3M/IOP/2022>, 2022b.
- Paatero, P. and Tapper, U.: Positive matrix factorization – a nonnegative factor model with optimal utilization of error-estimates of data values, *Environmetrics*, 5, 111–126, <https://doi.org/10.1002/env.3170050203>, 1994.
- Parrish, D. D., Kuster, W. C., Shao, M., Yokouchi, Y., Kondo, Y., Goldan, P. D., de Gouw, J. A., Koike, M., and Shirai, T.: Comparison of air pollutant emissions among mega-cities, *Atmos. Environ.*, 43, 6435–6441, <https://doi.org/10.1016/j.atmosenv.2009.06.024>, 2009.
- Quack, B. and Wallace, D. W. R.: Air-sea flux of bromoform: Controls, rates, and implications, *Glob. Biogeochem. Cycle*, 17, 1023, <https://doi.org/10.1029/2002GB001890>, 2003.
- Ratte, M., Plassdulmer, C., Koppmann, R., and Rudolph, J.: Horizontal and vertical profiles of light-hydrocarbons in seawater related to biological, chemical and physical parameters, *Tellus Ser. B-Chem. Phys. Meteorol.*, 47, 607–623, <https://doi.org/10.1034/j.1600-0889.47.issue5.8.x>, 1995.
- Ratte, M., Plassdulmer, C., Koppmann, R., Rudolph, J., and Denga, J.: Production mechanism of c₂-c₄ hydrocarbons in seawater – field-measurements and experiments, *Glob. Biogeochem. Cycle*, 7, 369–378, <https://doi.org/10.1029/93gb00054>, 1993.
- Riemer, D. D., Milne, P. J., Zika, R. G., and Pos, W. H.: Photo-production of nonmethane hydrocarbons (NMHCs) in seawater, *Mar. Chem.*, 71, 177–198, [https://doi.org/10.1016/S0304-4203\(00\)00048-7](https://doi.org/10.1016/S0304-4203(00)00048-7), 2000.
- Rossabi, S. and Helmig, D.: Changes in atmospheric butanes and pentanes and their isomeric ratios in the continental United States, *J. Geophys. Res.-Atmos.*, 123, 3772–3790, <https://doi.org/10.1002/2017JD027709>, 2018.
- Rudolph, J. and Johnen, F. J.: Measurements of light atmospheric hydrocarbons over the Atlantic in regions of low bi-

- ological activity, *J. Geophys. Res.-Atmos.*, 95, 20583–20591, <https://doi.org/10.1029/JD095iD12p20583>, 1990.
- Russo, R. S., Zhou, Y., White, M. L., Mao, H., Talbot, R., and Sive, B. C.: Multi-year (2004–2008) record of nonmethane hydrocarbons and halocarbons in New England: seasonal variations and regional sources, *Atmos. Chem. Phys.*, 10, 4909–4929, <https://doi.org/10.5194/acp-10-4909-2010>, 2010.
- Russo, R. S., Talbot, R. W., Dibb, J. E., Scheuer, E., Seid, G., Jordan, C. E., Fuelberg, H. E., Sachse, G. W., Avery, M. A., Vay, S. A., Blake, D. R., Blake, N. J., Atlas, E., Fried, A., Sandholm, S. T., Tan, D., Singh, H. B., Snow, J., and Heikes, B. G.: Chemical composition of Asian continental outflow over the Western Pacific: Results from Transport and Chemical Evolution over the Pacific (TRACE-P), *J. Geophys. Res.-Atmos.*, 108, 8804, <https://doi.org/10.1029/2002JD003184>, 2003.
- Sahu, L. K., Lal, S., and Venkataramani, S.: Impact of monsoon circulations on oceanic emissions of light alkenes over bay of Bengal, *Glob. Biogeochem. Cycle*, 24, GB4028, <https://doi.org/10.1029/2009GB003766>, 2010.
- Sahu, L. K., Lal, S., and Venkataramani, S.: Seasonality in the latitudinal distributions of NMHCs over bay of Bengal, *Atmos. Environ.*, 45, 2356–2366, <https://doi.org/10.1016/j.atmosenv.2011.02.021>, 2011.
- Schlitzer, R.: Ocean Data View, <https://odv.awi.de/> (last access: 30 May 2024), 2023.
- Solomon, S., Thompson, D. W. J., Portmann, R. W., Oltmans, S. J., and Thompson, A. M.: On the distribution and variability of ozone in the tropical upper troposphere: Implications for tropical deep convection and chemical-dynamical coupling, *Geophys. Res. Lett.*, 32, L23813, <https://doi.org/10.1029/2005GL024323>, 2005.
- Sindelarova, K., Granier, C., Bouarar, I., Guenther, A., Tilmes, S., Stavrou, T., Müller, J.-F., Kuhn, U., Stefani, P., and Knorr, W.: Global data set of biogenic VOC emissions calculated by the MEGAN model over the last 30 years, *Atmos. Chem. Phys.*, 14, 9317–9341, <https://doi.org/10.5194/acp-14-9317-2014>, 2014.
- Singh, H. and Zimmerman, P. B.: Atmospheric distribution and sources of nonmethane hydrocarbons, *Adv. Environ. Sci. Technol.*, 24, 177–235, <https://api.semanticscholar.org/CorpusID:129274915> (last access: 30 June 2023), 1992.
- Song, J. W., Zhang, Y. Y., Zhang, Y. L., Yuan, Q., Zhao, Y., Wang, X. M., Zou, S. C., Xu, W. H., and Lai, S. C.: A case study on the characterization of non-methane hydrocarbons over the South China Sea: Implication of land-sea air exchange, *Sci. Total Environ.*, 717, 134754, <https://doi.org/10.1016/j.scitotenv.2019.134754>, 2020.
- Song, Y., Shao, M., Liu, Y., Lu, S. H., Kuster, W., Goldan, P., and Xie, S. D.: Source apportionment of ambient volatile organic compounds in Beijing, *Environ. Sci. Technol.*, 41, 4348–4353, <https://doi.org/10.1021/es0625982>, 2007.
- Stein, A. F., Draxler, R. R., Rolph, G. D., Stunder, B. J., Cohen, B. M. D., and Ngan, F.: NOAA's HYSPLIT Atmospheric Transport and Dispersion Modeling System, *B. Am. Meteorol. Soc.*, 96, 2059–2077, <https://doi.org/10.1175/BAMS-D-14-00110.1>, 2015.
- Swarthout, R. F., Russo, R. S., Zhou, Y., Hart, A. H., and Sive, B. C.: Volatile organic compound distributions during the NACHTT campaign at the Boulder Atmospheric Observatory: Influence of urban and natural gas sources, *J. Geophys. Res.-Atmos.*, 118, 10614–610637, <https://doi.org/10.1002/jgrd.50722>, 2013.
- Talbot, R., Dibb, J., Scheuer, E., Seid, G., Russo, R., Sandholm, S., Tan, D., Singh, H., Blake, D., Blake, N., Atlas, E., Sachse, G., Jordan, C., and Avery, M.: Reactive nitrogen in Asian continental outflow over the western Pacific: Results from the NASA Transport and Chemical Evolution over the Pacific (TRACE-P) airborne mission, *J. Geophys. Res.-Atmos.*, 108, 8803, <https://doi.org/10.1029/2002JD003129>, 2003.
- Tang, J. H., Chan, L. Y., Chang, C. C., Liu, S., and Li, Y. S.: Characteristics and sources of non-methane hydrocarbons in background atmospheres of eastern, southwestern, and southern China, *J. Geophys. Res.-Atmos.*, 114, D03304, <https://doi.org/10.1029/2008JD010333>, 2009.
- Tran, S., Bonsang, B., Gros, V., Peeken, I., Sarda-Esteve, R., Bernhardt, A., and Belviso, S.: A survey of carbon monoxide and non-methane hydrocarbons in the Arctic Ocean during summer 2010, *Biogeosciences*, 10, 1909–1935, <https://doi.org/10.5194/bg-10-1909-2013>, 2013.
- Tsai, W. Y., Chan, L. Y., Blake, D. R., and Chu, K. W.: Vehicular fuel composition and atmospheric emissions in South China: Hong Kong, Macau, Guangzhou, and Zhuhai, *Atmos. Chem. Phys.*, 6, 3281–3288, <https://doi.org/10.5194/acp-6-3281-2006>, 2006.
- Wang, J.: Dataset of “Roles of oceanic ventilation and terrestrial outflow in the atmospheric non-methane hydrocarbons over the Chinese marginal seas”, Figshare [data set], <https://doi.org/10.6084/m9.figshare.24722286.v1>, 2023.
- Wang, J.: Matlab code for RL calculation, Figshare [code], <https://doi.org/10.6084/m9.figshare.26499985>, 2024.
- Wang, T., Ding, A. J., Blake, D. R., Zahorowski, W., Poon, C. N., and Li, Y. S.: Chemical characterization of the boundary layer outflow of air pollution to Hong Kong during february-april 2001, *J. Geophys. Res.-Atmos.*, 108, 8787, <https://doi.org/10.1029/2002JD003272>, 2003.
- Wang, T., Guo, H., Blake, D. R., Kwok, Y. H., Simpson, I. J., and Li, Y. S.: Measurements of trace gases in the inflow of South China Sea background air and outflow of regional pollution at Tai O, Southern China, *J. Atmos. Chem.*, 52, 295–317, <https://doi.org/10.1007/s10874-005-2219-x>, 2005.
- Wanninkhof, R.: Relationship between wind-speed and gas-exchange over the ocean, *J. Geophys. Res.-Oceans*, 97, 7373–7382, <https://doi.org/10.1029/92jc00188>, 1992.
- Warneke, C. and de Gouw, J. A.: Organic trace gas composition of the marine boundary layer over the Northwest Indian Ocean in april 2000, *Atmos. Environ.*, 35, 5923–5933, [https://doi.org/10.1016/S1352-2310\(01\)00384-3](https://doi.org/10.1016/S1352-2310(01)00384-3), 2001.
- Wessel, P. and Smith W. H. F.: A global, self-consistent, hierarchical, high-resolution shoreline database, *J. Geophys. Res.*, 101, 8741–8743, <https://doi.org/10.1029/96JB00104>, 1996.
- Wilke, C. R. and Chang, P.: Correlation of diffusion coefficients in dilute solutions, *AICHE Journal*, 1, 264–270, <https://doi.org/10.1002/aic.690010222>, 1955.
- Willis, M. D., Köllner, F., Burkart, J., Bozem, H., Thomas, J. L., Schneider, J., Aliabadi, A. A., Hoor, P. M., Schulz, H., Herber, A. B., Leaitch, W. R., and Abbatt, J. P. D.: Evidence for marine biogenic influence on summertime arctic aerosol, *Geophys. Res. Lett.*, 44, 6460–6470, <https://doi.org/10.1002/2017GL073359>, 2017.

- Wong, H. L. A., Wang, T., Ding, A., Blake, D. R., and Nam, J. C.: Impact of Asian continental outflow on the concentrations of O₃, CO, NMHCs and halocarbons on Jeju Island, South Korea during march 2005, *Atmos. Environ.*, 41, 2933–2944, <https://doi.org/10.1016/j.atmosenv.2006.12.030>, 2007.
- Wu, D., Ding, X., Li, Q., Sun, J., Huang, C., Yao, L., Wang, X., Ye, X., Chen, Y., He, H., and Chen, J.: Pollutants emitted from typical Chinese vessels: Potential contributions to ozone and secondary organic aerosols, *J. Clean. Prod.*, 238, 117862, <https://doi.org/10.1016/j.jclepro.2019.117862>, 2019.
- Wu, F., Yu, Y., Sun, J., Zhang, J., Wang, J., Tang, G., and Wang, Y.: Characteristics, source apportionment and reactivity of ambient volatile organic compounds at Dinghu Mountain in Guangdong Province, China, *Sci. Total Environ.*, 548–549, 347–359, <https://doi.org/10.1016/j.scitotenv.2015.11.069>, 2016.
- Wu, R. R. and Xie, S. D.: Spatial distribution of secondary organic aerosol formation potential in China derived from speciated anthropogenic volatile organic compound emissions, *Environ. Sci. Technol.*, 52, 8146–8156, <https://doi.org/10.1021/acs.est.8b01269>, 2018.
- Wu, Y. C., Li, J. L., Wang, J., Zhuang, G. C., Liu, X. T., Zhang, H. H., and Yang, G. P.: Occurrence, emission and environmental effects of non-methane hydrocarbons in the Yellow Sea and the East China Sea, *Environ. Pollut.*, 270, 12, <https://doi.org/10.1016/j.envpol.2020.116305>, 2021.
- Wu, Y. C., Gao, X. X., Zhang, H. H., Liu, Y. Z., Wang, J., Xu, F., Zhang, G. L., and Chen, Z. H.: Characteristics and emissions of isoprene and other non-methane hydrocarbons in the Northwest Pacific Ocean and responses to atmospheric aerosol deposition, *Sci. Total Environ.*, 876, 162808, <https://doi.org/10.1016/j.scitotenv.2023.162808>, 2023.
- Xiao, Q., Li, M., Liu, H., Fu, M., Deng, F., Lv, Z., Man, H., Jin, X., Liu, S., and He, K.: Characteristics of marine shipping emissions at berth: profiles for particulate matter and volatile organic compounds, *Atmos. Chem. Phys.*, 18, 9527–9545, <https://doi.org/10.5194/acp-18-9527-2018>, 2018a.
- Xiao, Q., Li, M., Liu, H., Fu, M., Deng, F., Lv, Z., Man, H., Jin, X., Liu, S., and He, K.: Characteristics of marine shipping emissions at berth: profiles for particulate matter and volatile organic compounds, *Atmos. Chem. Phys.*, 18, 9527–9545, <https://doi.org/10.5194/acp-18-9527-2018>, 2018b.
- Xu, G. B., Xu, F., Ji, X., Zhang, J., Yan, S. B., Mao, S. H., Yang, G. P.: Carbon monoxide cycling in the Eastern Indian Ocean, *J. Geophys. Res.-Oceans*, 128, e2022JC019411, <https://doi.org/10.1029/2022JC019411>.
- Yuan, Q., Lai, S. C., Song, J. W., Ding, X., Zheng, L. S., Wang, X. M., Zhao, Y., Zheng, J. Y., Yue, D. L., Zhong, L. J., Niu, X. J., and Zhang, Y. Y.: Seasonal cycles of secondary organic aerosol tracers in rural Guangzhou, Southern China: The importance of atmospheric oxidants, *Environ. Pollut.*, 240, 884–893, <https://doi.org/10.1016/j.envpol.2018.05.009>, 2018.
- Zhang, Y., Zhi, Z., Li, X., Gao, J., and Song, Y.: Carboxylated mesoporous carbon microparticles as new approach to improve the oral bioavailability of poorly water-soluble carvedilol, *Int. J. Pharm.*, 454, 403–411, <https://doi.org/10.1016/j.ijpharm.2013.07.009>, 2013.
- Zhang, Y., Wang, X., Zhang, Z., Lü, S., Huang, Z., and Li, L.: Sources of c₂–c₄ alkenes, the most important ozone nonmethane hydrocarbon precursors in the Pearl River Delta region, *Sci. Total Environ.*, 502, 236–245, <https://doi.org/10.1016/j.scitotenv.2014.09.024>, 2015.
- Zhang, Z., Zhang, Y., Wang, X., Lü, S., Huang, Z., Huang, X., Yang, W., Wang, Y., and Zhang, Q.: Spatiotemporal patterns and source implications of aromatic hydrocarbons at six rural sites across China's developed coastal regions, *J. Geophys. Res.-Atmos.*, 121, 6669–6687, <https://doi.org/10.1002/2016JD025115>, 2016.
- Zhang, Z. J., Yan, X. Y., Gao, F. L., Thai, P., Wang, H., Chen, D., Zhou, L., Gong, D. C., Li, Q. Q., Morawska, L., and Wang, B. G.: Emission and health risk assessment of volatile organic compounds in various processes of a petroleum refinery in the Pearl River Delta, China, *Environ. Pollut.*, 238, 452–461, <https://doi.org/10.1016/j.envpol.2018.03.054>, 2018.
- Zhou, S. Q., Chen, Y., Paytan, A., Li, H. W., Wang, F. H., Zhu, Y. C., Yang, T. J., Zhang, Y., and Zhang, R. F.: Non-marine sources contribute to aerosol methanesulfonate over coastal seas, *J. Geophys. Res.-Atmos.*, 126, e2021JD034960, <https://doi.org/10.1029/2021JD034960>, 2021.
- Zou, Y. W., He, Z., Liu, C. Y., Qi, Q. Q., Yang, G. P., and Mao, S. H.: Coastal observation of halocarbons in the yellow sea and east china sea during winter: Spatial distribution and influence of different factors on the enzyme-mediated reactions, *Environ. Pollut.*, 290, 118022, <https://doi.org/10.1016/j.envpol.2021.118022>, 2021.